Contents

Chapter 1

Wire Antenna modeling

The purpose of this chapter is to give a brief introduction to simple modeling of wire antenna structures. The approach is to model the antenna in the circuit domain as a common transmission line structure in order to obtain a current distribution estimate. The wave domain model is based on the assumption, that the wire antenna structure can be considered as a finite number of infinitesimal dipole (Hertz dipole) radiators with respect to the radiated fields. All the individual field contributions from each Hertz dipole are determined by utilizing the current distribution obtained from the circuit domain model. Finally, the total field is calculated as a simple sum of all these contributions. Since a wire antenna structure can be quite complex with respect to geometry, some level of coordinate transformation is needed in order to obtain the correct vector sum in each point in space. The circuit domain model is not covered in this chapter - the focus is on the wave domain part.

1.1 Analysis

Two distinct principles exist to calculate the radiated far field from a wire antenna structure: (1) using theory of retarded potentials based on knowledge of the surface current distribution to calculate E-field or (2) solving Maxwell's equations numerically to estimate E-field in a volume containing the structure and a radiating media, e.g. air, and then apply the Fourier transform to the aperture E-field on the boundaries to find the far field radiation properties. The latter principle involves making a complete 3D model of the total PCB structure including the antenna, extracting a suitable mesh and then do the calculations. Typically, this is done by the use of a specialized program, e.g. HFSS from Ansoft or CST from CST. However, if it is feasible to do a decent estimation of the current distribution, the first principle is far simpler at the expense of accuracy and level of detail.

The total radiated fields is calculated by utilizing the division of the wire antenna geometry into into small segments with a length of h that obey the requirement $h \ll \lambda$. It is assumed that the size of the segments justify the use of a uniform current dis-

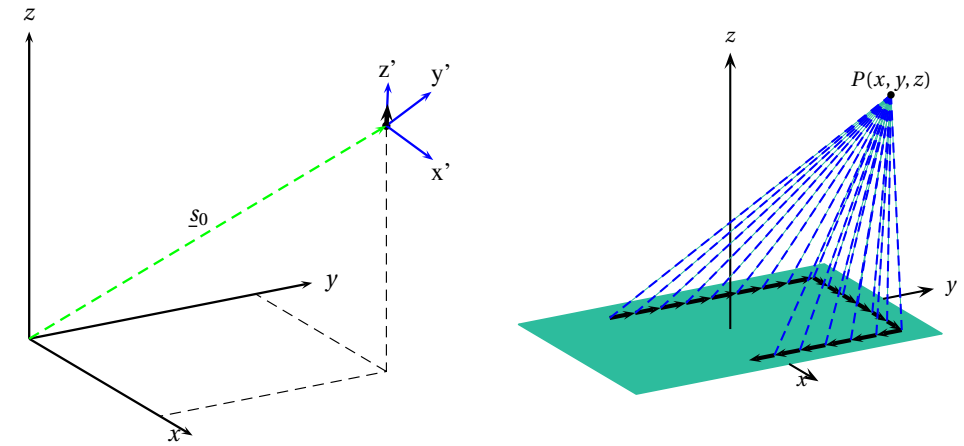

(a) Illustration of the basic Hertz dipole setup.

(b) Example wire antenna geometry divided in Hertz dipoles

Figure 1.1: Illustration of the Hertz dipole setup. (a) An arbitrary placement of a Hertz dipole has been chosen and the placement of the local coordinate system in the global coordinate system (*x,y,z*) is indicated. The Hertz dipole itself is depicted as a black vector. (b) The division of an example wire antenna geometry into a number of Hertz dipoles is illustrated. The direction vectors to the observer point $P(x, y, z)$ are indicated with dashed blue lines.

tribution on each segment. All the segments are then considered to be Hertz dipoles and each of these dipoles contribute to the electromagnetic field in every point in space. The challenge is then to determine all contributions and add them together, respecting the vectorial nature of the calculation. The details of the calculation are described in the following.

It is necessary to establish the relationsship between the uniform current distribution ($I(z)=I_0$) and the radiated electromagnetic field for the Hertz dipole. A Hertz dipole placed in (0,0,0) in the local *(x',y',z')* coordinate system with the dipole axis aligned with the z'-axis radiates the electric and magnetic field stated in equation 1.1 with the local coordinate system as reference. An illustration of the Hertz dipole setup is shown in figure 1.1. Here, an arbitrary placement of a Hertz dipole has been chosen and the placement of the local coordinate system in the global coordinate system (*(x,y,z)*) is indicated. The Hertz dipole itself is depicted as a black vector. The expressions provided here are only valid when the dipole length (h) is much smaller than the wavelength ($h \ll \lambda$) and the current distribution is uniform.

$$\underline{\underline{E}} = \begin{bmatrix} E_r \\ E_\theta \\ E_\phi \end{bmatrix} = \begin{bmatrix} \eta \frac{I_0 h \cos\theta}{2\pi r^2} \left(1 + \frac{1}{jkr}\right) e^{-jkr} \\ j\eta \frac{kI_0 h \sin\theta}{4\pi r} \left(1 + \frac{1}{jkr} - \frac{1}{(kr)^2}\right) e^{-jkr} \\ 0 \end{bmatrix}$$
$$\underline{\underline{H}} = \begin{bmatrix} H_r \\ H_\theta \\ H_\phi \end{bmatrix} = \begin{bmatrix} 0 \\ 0 \\ j \frac{kI_0 h \sin\theta}{4\pi r} \left(1 + \frac{1}{jkr}\right) e^{-jkr} \end{bmatrix} \tag{1.1}$$

The complexity of the geometry of the setup is illustrated in figure 1.1. Here, an example PCB track is divided into a number of small Hertz dipoles and only one observer point in space is considered (x_p, y_p, z_p). The challenge is now to determine the contributions from all Hertz dipoles in this point in vector form. Since the radiated field from every Hertz dipole is dependent on the distance to the point (*R'*) and the angle between the dipole axis normal vector ($\underline{\hat{h}}$) and the normalized direction vector from the position of the Hertz dipole to the observer point ($\underline{\hat{s}}$), it is necessary to perform some vector manipulation in order to obtain each contribution on vector form. Basically, it is required to find the direction of the E_r, E_θ and H_ϕ contributions and their magnitude. Each of these contributions are represented by a normalized vector in the global coordinate system: $\underline{\hat{r}}$, $\underline{\hat{\theta}}$ and $\underline{\hat{\phi}}$. The derivation of expressions for the normal vectors is found in equation 1.2.

$$\begin{aligned}
\underline{\hat{r}} &= \frac{\underline{s}}{\|\underline{s}\|} = \underline{\hat{s}} \\
\underline{\hat{\phi}} &= \frac{\underline{\hat{h}} \times \underline{\hat{s}}}{\|\underline{\hat{h}} \times \underline{\hat{s}}\|} \\
\underline{\hat{\theta}} &= \frac{\underline{\hat{\phi}} \times \underline{\hat{s}}}{\left\|\underline{\hat{\phi}} \times \underline{\hat{s}}\right\|} = \frac{(\underline{\hat{h}} \times \underline{\hat{s}}) \times \underline{\hat{s}}}{\|(\underline{\hat{h}} \times \underline{\hat{s}}) \times \underline{\hat{s}}\|} = -\frac{\underline{\hat{s}} \times (\underline{\hat{h}} \times \underline{\hat{s}})}{\|\underline{\hat{s}} \times (\underline{\hat{h}} \times \underline{\hat{s}})\|} \\
&= \frac{-(\underline{\hat{h}}(\underline{\hat{s}} \cdot \underline{\hat{s}}) - \underline{\hat{s}}(\underline{\hat{s}} \cdot \underline{\hat{h}}))}{\|-(\underline{\hat{h}}(\underline{\hat{s}} \cdot \underline{\hat{s}}) - \underline{\hat{s}}(\underline{\hat{s}} \cdot \underline{\hat{h}}))\|} = \frac{(\underline{\hat{s}} \cdot \underline{\hat{h}})\underline{\hat{s}} - \underline{\hat{h}}}{\|(\underline{\hat{s}} \cdot \underline{\hat{h}})\underline{\hat{s}} - \underline{\hat{h}}\|}
\end{aligned} \tag{1.2}$$

Although the electromagnetic field is described using spherical local coordinates, all vectors in equation 1.2 are cartesian representations using the global coordinate system. This eliminates the need for a two-step process with separate transformation from spherical to cartesian coordinates in the local coordinate system followed by a transformation from local to global coordinates.

Calculation of the magnitude of the field contributions from each Hertz dipole is

based on the current distribution (I_0), the length of the individual segment (h), the distance to the observer point (R') and the spherical coordinate, θ. Assuming that we can estimate the current distribution by means of the circuit model, only the latter two entities are unknown variables. However, they are easily derived from the geometry of the setup. The derivation can be found in equation 1.3.

$$\begin{aligned} R' &= \left\| \underline{s} \right\| \\ \begin{cases} \left\| \hat{\underline{h}} \times \hat{\underline{s}} \right\| &= \left\| \hat{\underline{h}} \right\| \left\| \hat{\underline{s}} \right\| \sin\theta = \sin\theta \\ \hat{\underline{s}} \cdot \hat{\underline{h}} &= \left\| \hat{\underline{s}} \right\| \left\| \hat{\underline{h}} \right\| \cos\theta = \cos\theta \end{cases} \end{aligned} \tag{1.3}$$

Please note, that the angle is not explicitly determined. The reason is that only $\cos\theta$ and $\sin\theta$ is required for the electromagnetic field calculations. Due to the fact, that it is more convenient to express the fields in sperical coordinates, a final coordinate transformation from cartesian to spherical coordinates is required. This transformation is stated for completeness in equation 1.4 for an arbitrary vector ($\underline{V}$)

$$\underline{V}_{r\theta\phi} = \begin{bmatrix} V_r \\ V_\theta \\ V_\phi \end{bmatrix} = \begin{bmatrix} \sin\theta\cos\phi & \sin\theta\sin\phi & +\cos\theta \\ \cos\theta\cos\phi & \cos\theta\sin\phi & -\sin\theta \\ -\sin\phi & \cos\phi & 0 \end{bmatrix} \begin{bmatrix} V_x \\ V_y \\ V_z \end{bmatrix} \tag{1.4}$$

The derivation of the peak directivity can be based directly on the fundamental directivity definition ([1]). The result of doing so is shown in equation 1.6.

$$\begin{aligned} D_0 &= \frac{\left\| \underline{S} \right\|_{max}}{\left\| \underline{S} \right\|_{avg}} = \frac{\left\| \underline{S} \right\|_{max}}{\frac{P_{rad}}{4\pi r^2}} = 4\pi r^2 \frac{\left\| \underline{S} \right\|_{max}}{P_{rad}} \\ &= 4\pi r^2 \frac{\left\| \underline{S} \right\|_{max}}{\sum_{\text{surface}} \frac{1}{2}\mathrm{Re}\left\{ \underline{E} \times \underline{H}^* \right\} r^2 \sin\theta \Delta\phi \Delta\theta} \qquad (1.5) \\ &= \frac{8\pi}{\Delta\phi\Delta\theta} \frac{\left\| \underline{S} \right\|_{max}}{\sum_{\text{surface}} \mathrm{Re}\left\{ \underline{E} \times \underline{H}^* \right\} \sin\theta} \qquad (1.6) \end{aligned}$$

All calculations of radiated power contributions required to determine directivity are based on the radial part of Poynting's vector in realtime average power form (S_r). This is illustrated in equation 1.7. The equation shows the peak power expression.

$$\underline{S} = \begin{bmatrix} S_r \\ S_\theta \\ S_\phi \end{bmatrix} = \frac{1}{2}\mathrm{Re}\left\{ \underline{E} \times \underline{H}^* \right\} \qquad \Rightarrow \qquad S_r = \frac{1}{2}\mathrm{Re}\left\{ E_\theta \cdot H_\phi^* - E_\phi \cdot H_\theta^* \right\} \tag{1.7}$$

Chapter 2

Antenna interfacing

A brief introduction to the art of antenna interfacing is presented in this chapter. This includes basic S-parameter theory and classic matching circuit topologies. The reader is assumed to be familiar with the definition and use of the Smith chart for impedance match purposes. An introduction to this type of chart is available in Appendix B.

2.1 S-parameters

bla

2.2 Matching networks

bla

2.3 Examples

bla

2.3.1 b λ/2 dipole

bla

Appendices

Appendix A

Anechoic Chamber

This appendix contains a brief description of the anechoic chamber and performance related parameters.

A.1 Anechoic chamber setup

An illustration of the anechoic chamber measurement setup is provided in figure A.1 together with a view of the antenna mounted in the chamber.

The distance (d) between the reference antenna and the DUT is 5 m.

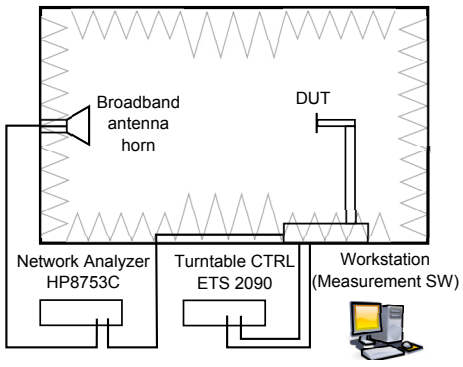

(a) Anechoic chamber setup

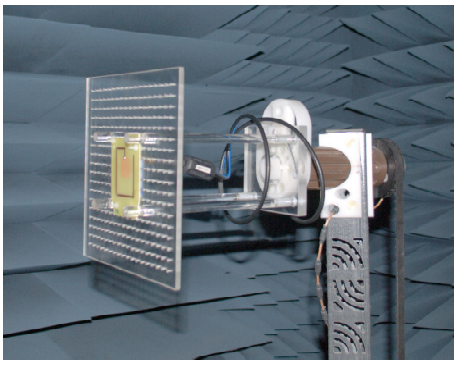

(b) Antenna and mounting structure

Figure A.1: (a) An illustration of the anechoic chamber setup. The computer is equipped with software to control the network analyzer, the turntable controller and a polarisation switch (Agilent N1810UL) (not shown!). A broadband reference antenna horn (ETS 3164-04) is mounted on the end wall (left). (b) A picture of the actual mounting of the antenna on the turntable tower inside the anechoic room.

f (MHz)	Gain (dBi)	Cross-polarisation suppression (dB)	VSWR (-)	Mismatch loss (dB)
433	0.5	>20	2.5	0.9
868	5.5	>20	2.0	0.5
2450	9.5	>20	2.2	0.7

Table A.1: Data for ETS-Lindgren dual polarized horn of type ETS 3164-04 at three frequencies. The data for 433 MHz has been estimated by means of extrapolating the data found in [2].

A.1.1 Dual polarized horn - ETS 3164-04

Although the lower frequency limit of the horn is specified to approx. 700 MHz, it can be used at 433 MHz but strongly reduced performance should be anticipated. According to the information found in ETS-Lindgrens dual polarized horn manual [2], cross-polarisation at 433 MHz is estimated to suppressed approx 20 dB. VSWR is estimated to be approx. 2.5, corresponding to an extra path loss of 0.9 dB (mismatch loss). Extrapolation of the gain leads to an estimate of approx. 0.5 dBi. Data for the three frequency bands is summarized in table A.1.

A.1.2 Cables

Two types of cable are present in the measurement setup: Huber+Suhner Enviroflex-316 [3] and S_04272 [4] . The two cables are referenced as cable 1 (C1) and cable 2 (C2) in the text. Expression to calculate the nominal attenuation (in dB/m) for Enviroflex-316 is given in equation A.1. A similar expression for S_04272 is given in equation A.2. It should be noted, that the frequency has to be entered in GHz in both these expressions.

$$\alpha_{C1} = 0.812\sqrt{f} + 0.1504f \qquad [\text{dB/m}] \tag{A.1}$$

$$\alpha_{C2} = 0.197\sqrt{f} + 0.045f \qquad [\text{dB/m}] \tag{A.2}$$

Length of C1 is approx. 6 m and length of C2 is approx. 15 m. An extra 4 m of cable is inside the anechoic chamber. The performance of this length of cable is approx. the same as C1. Therefore, a total of 10 m of C1 is assumed to be present in the setup. This leads to the cable attenuation at the three center frequencies listed in table A.2

A.1.3 Polarisation switch - Agilent N1810UL

An insertion loss expression for the polarisation switch (L_P) is available in the datasheet ([5]). The expression is shown in equation A.3. Again, f is required to be entered in GHz.

f (MHz)	L_{C1} (dB)	L_{C2} (dB)	L_C (dB)	L_P (dB)	L_0 (dB)	L_{TOT} (dB)
433	6.0	2.2	8.2	0.4	39.2	48.2
868	8.9	3.3	12.2	0.4	45.2	52.8
2450	16.4	6.3	22.7	0.4	54.2	68.5

Table A.2: Cable losses (L_{C1}, L_{C2} and L_C) , polarisation switch loss, free space loss (L_0) and total loss (L_{TOT}) at the three center frequencies.

$$L_P = 0.35 + \frac{0.45}{26.5} f \qquad [\text{dB}] \tag{A.3}$$

Table A.2 lists the insertion loss at the three center frequencies.

A.1.4 Free space loss

The free space loss in the anechoic chamber is determined from Friis' free space transmission formula ([1], chapter 2). The free space loss (L_0) calculation is shown in equation A.4:

$$L_0 = 10\log\left(\left(\frac{4\pi d}{\lambda}\right)^2\right) = 20\log\left(\frac{4\pi d}{\lambda}\right) = 20\log\left(\frac{4\pi d f}{c}\right) \tag{A.4}$$

A table listing of the free space loss associated with the three center frequencies is shown in table A.2

A.1.5 Total path loss

The difference between the combined losses and the horn antenna gain represents the total loss (L_{TOT}) associated with the anechoic chamber setup. This loss is calculated and listed in table A.2. Here, the potential mismatch in connection with the reference horn antenna has been included.

A.1.6 Gain

Based on the total loss from the previous section, it is possible to evaluate the gain of the DUT (G_{DUT}). The expression is given in equation A.5.

$$G_{DUT} = \left|S_{21}\right| + L_{TOT} \qquad [\text{dB}] \tag{A.5}$$

This is a simple rearrangement of Friis' free space transmission formula with $\left|S_{21}\right|$ substituting the ratio between received and transmitted power. Note that the reference horn antenna gain is included in the total loss (L_{TOT}). Both $\left|S_{21}\right|$ and the total loss should be entered in dB as indicated in the expression. The resulting gain (G_{DUT}) is in dBi.

Appendix B

Smith chart

Bibliography

[1] C. Balanis, *Antenna Theory: Analysis and Design*. Wiley, 2005.

[2] ETS-Lindgren, "Dual polarized horns - manual," ETS-Lindgren website, ETS-Lindgren, April 2005, http://www.ets-lindgren.com.

[3] HUBER+SUHNER, "Datasheet: Coaxial Cable: ENVIROFLEX_316," HUBER+SUHNER website, HUBER+SUHNER, http://www.hubersuhner.com.

[4] ——, "Datasheet: Coaxial Cable: S_04272_B," HUBER+SUHNER website, HUBER+SUHNER, http://www.hubersuhner.com.

[5] A. Technologies, "Agilent N1810/1/2 Coaxial Switches," Agilent Technologies website, Agilent Technologies, 2011, http://www.Agilent.com.